INTERNATIONAL JOURNAL FOR NUMERICAL METHODS IN ENGINEERING
*Int. J. Numer. Meth. Engng.* **45**, 1607–1630 (1999)

# FINITE ELEMENT FORMULATION OF EXACT NON-REFLECTING BOUNDARY CONDITIONS FOR THE TIME-DEPENDENT WAVE EQUATION

LONNY L. THOMPSON[1,*,†] AND RUNNONG HUAN[2,‡]

[1] *Advanced Computational Mechanics Laboratory, Clemson University, Clemson, SC 29634, U.S.A.*
[2] *Department of Mechanical Engineering, Clemson University, Clemson, SC 29634, U.S.A.*

## SUMMARY

A modified version of an exact Non-reflecting Boundary Condition (NRBC) first derived by Grote and Keller is implemented in a finite element formulation for the scalar wave equation. The NRBC annihilate the first $N$ wave harmonics on a spherical truncation boundary, and may be viewed as an extension of the second-order local boundary condition derived by Bayliss and Turkel. Two alternative finite element formulations are given. In the first, the boundary operator is implemented directly as a 'natural' boundary condition in the weak form of the initial–boundary value problem. In the second, the operator is implemented indirectly by introducing auxiliary variables on the truncation boundary. Several versions of implicit and explicit time-integration schemes are presented for solution of the finite element semidiscrete equations concurrently with the first-order differential equations associated with the NRBC and an auxiliary variable. Numerical studies are performed to assess the accuracy and convergence properties of the NRBC when implemented in the finite element method. The results demonstrate that the finite element formulation of the (modified) NRBC is remarkably robust, and highly accurate. Copyright © 1999 John Wiley & Sons, Ltd.

KEY WORDS: non-reflecting boundary conditions, wave equation, finite element method, wave propagation

## 1. INTRODUCTION

When the finite element method is used to model the wave equation in infinite domains, accurate absorbing boundary conditions, infinite elements, or absorbing layers, are required on an artificial truncation boundary $\Gamma$ that surrounds the source of radiation or scattering [1]. If the form of the boundary treatment is over-simplified, spurious reflected waves can be generated at the artificial boundary, which can substantially degrade the accuracy of the numerical solution. For example, a standard approach is to apply local (differential) boundary operators on $\Gamma$ which annihilate leading terms in the radial expansion for outgoing wave solutions. A well-known sequence of boundary conditions applied to a spherical boundary $\Gamma$ are the local operators derived by Bayliss

* Correspondence to: Lonny L. Thompson, Department of Mechanical Engineering, Clemson University, 102 Fluor Daniel Engineering Building, Box 340921, Clemson, SC 29634-0921, U.S.A. E-mail: lonny.thompson@ces.clemson.edu
† Assistant Professor of Mechanical Engineering and Engineering Mechanics
‡ Graduate Research Assistant

Contract/grant sponsor: NSF

CCC 0029-5981/99/231607–24$17.50

*Received 17 August 1998*
*Revised 23 November 1998*

and Turkel [2]. The first two boundary conditions in this sequence are:

$$B_1\phi = \left(\frac{\partial}{\partial r} + \frac{1}{c}\frac{\partial}{\partial t} + \frac{1}{r}\right)\phi = 0 \tag{1}$$

$$B_2\phi = \left(\frac{\partial}{\partial r} + \frac{1}{c}\frac{\partial}{\partial t} + \frac{3}{r}\right)\left(\frac{\partial}{\partial r} + \frac{1}{c}\frac{\partial}{\partial t} + \frac{1}{r}\right)\phi = 0 \tag{2}$$

where $\phi(\mathbf{x}, t)$ is the solution to the scalar wave equation, $c$ is the wave speed, and $r$ is evaluated at radius $R$, of a spherical artificial boundary $\Gamma$. The boundary condition (1) is exact for a uniform spherical wave, while (2) is exact for both the first (spherical) and second harmonic for outgoing waves. While these boundary conditions are exact for lower modes, they exhibit significant spurious reflection for higher-order wave harmonics, especially as the position of $\Gamma$ approaches the source of radiation or scattering [3], and for low-frequency (long wavelength) components [4].

Recently, Grote and Keller [5, 6] have derived a sequence of non-reflecting boundary conditions for the wave equation

$$B_1\phi + \frac{1}{R}\sum_{n=1}^{\infty}\sum_{m=-n}^{n} \mathbf{e}_n \cdot \mathbf{z}_{nm}(t)\, Y_{nm}(\theta, \varphi) = 0 \tag{3}$$

$$B_2\phi - \frac{1}{R}\sum_{n=2}^{\infty}\sum_{m=-n}^{n} \tilde{\mathbf{e}}_n \cdot \mathbf{z}_{nm}(t)\, Y_{nm}(\theta, \varphi) = 0 \tag{4}$$

where $Y_{nm}$ are spherical harmonics, $\mathbf{e}_n$, $\tilde{\mathbf{e}}_n$, are vectors of coefficients, and $\mathbf{z}_{nm}(t)$ are solutions to a first-order system of ordinary differential equations driven by the radial harmonics $\phi_{nm} = (\phi, Y_{nm})_\Gamma$.

The summation over the series in (3) and (4) may be viewed as extensions of the local $B_1$ and $B_2$ operators of Bayliss and Turkel [2] respectively. In computation, the sum over $n$ in (3) and (4) is truncated at an arbitrary value $N \geqslant 1$, and $N \geqslant 2$, respectively. Both boundary conditions are exact for modes $n \leqslant N$. For modes $n > N$, (3) reduces to (1) while (4) reduces to (2). Therefore, when truncated at a finite value $N$, boundary condition (4) is expected to approximate the modes $n > N$ with greater accuracy than (3).

The implementation of (3) and (4) using finite difference methods is discussed in [6]. In [7, 8] we implemented a modified version of (3) in a standard semidiscrete finite element formulation with several alternative implicit and explicit time-integrators. In this paper we show how to implement the NRBC (4) in the finite element method. To use (4) in a finite element formulation, we reformulate the boundary condition and derive an equivalent but more tractable form, which does not involve high-order radial derivatives. Two alternative formulations are given. In the first, the boundary operator is implemented directly as a 'natural' boundary condition in the variational equation. In the second, the operator is implemented indirectly by introducing auxiliary variables on the nonreflecting boundary $\Gamma$. The indirect implementation leads to a symmetric system of matrix equations, and avoids the unsymmetric damping matrix present in the direct implementation, albeit at the expense of solving for additional unknowns on $\Gamma$. Several versions of implicit and explicit time-integration schemes are presented for solution of the finite element semidiscrete equations concurrently with the first-order differential equations associated with the non-reflecting boundary condition and an auxiliary variable.

Numerical studies are performed for a challenging test problem of radiation from a piston on a sphere, to assess the accuracy and convergence properties of the nonreflecting boundary conditions when implemented in the finite element method. We compare the evolution of the direct and indirect approaches to formulating (4) in the finite element method using an $L_2$ error norm. We

 

then compare the behaviour of the finite element formulations of the NRBC (3) and (4) as a function of the number of terms $N$ used in the series and the radial distance from the radiator to the truncation boundary where they are imposed. Finally, the effect of frequency on the behaviour of the non-reflecting boundary conditions is investigated.

## 2. EXACT NON-REFLECTING BOUNDARY CONDITION

We consider time-dependent scattering/radiation in an infinite three-dimensional region. The unbounded region is truncated by a spherical boundary $\Gamma$, of radius $R$. We then denote by $\Omega$ the finite computational domain surrounded by $\Gamma$. Within $\Omega$ we assume the solution $\phi(\mathbf{x},t)$ is governed by the non-homogeneous wave equation:

$$\nabla^2\phi - \frac{1}{c^2}\frac{\partial^2\phi}{\partial t^2} = -f \quad \text{in } \Omega\times]0,T[ \tag{5}$$

$$\phi(\mathbf{x},0) = \phi_0, \quad \dot{\phi}(\mathbf{x},0) = \dot{\phi}_0, \quad \mathbf{x}\in\Omega \tag{6}$$

At $t=0$, the source $f(\mathbf{x},t)$ and initial data are assumed to be confined to the region $\Omega$, so that in the exterior domain $\mathscr{D}$, i.e., the region outside $\Gamma$, the scalar field $\phi(\mathbf{x},t)$ satisfies the homogeneous form of the wave equation,

$$\nabla^2\phi - \frac{1}{c^2}\frac{\partial^2\phi}{\partial t^2} = 0 \quad \text{in } \mathscr{D}\times]0,T[ \tag{7}$$

$$\phi(\mathbf{x},0) = 0, \quad \dot{\phi}(\mathbf{x},0) = 0, \quad \mathbf{x}\in\mathscr{D} \tag{8}$$

A general solution to (7) in spherical co-ordinates $(r,\theta,\varphi)$ is

$$\phi(r,\theta,\varphi,t) = \sum_{n=0}^{\infty}\sum_{m=-n}^{n}\phi_{nm}(r,t)Y_{nm}(\theta,\varphi) \tag{9}$$

where $Y_{nm}$ are orthogonal spherical harmonics normalized on the unit sphere given by,

$$Y_{nm}(\theta,\varphi) = [(2n+1)(n-|m|)!/4\pi(n+|m|)!]^{1/2}\mathrm{e}^{\mathrm{i}m\varphi}P_n^{|m|}(\cos\theta) \tag{10}$$

and $\phi_{nm}(r,t)$ are time-dependent radial functions.

As shown in [8], the exact non-reflecting boundary condition first derived in [5], may be obtained directly from recursive use of a relation for the radial functions given by Lamb [9]. In the following, we outline the derivation of two alternative forms of the NRBC (3) and (4).

The key result from [9] is the relation between the radial functions $\phi_{nm}$ given by

$$\phi_{nm} = \left(\frac{\partial}{\partial r} - \frac{n-1}{r}\right)\phi_{n-1,m} \tag{11}$$

Recursive use of (11) leads to the result given in [8]

$$\phi_{nm} = \prod_{j=1}^{n}\left(\frac{\partial}{\partial r} - \frac{j-1}{r}\right)\phi_{00} \tag{12}$$

 

where the radial function $\phi_{00}(r,t)$ satisfies the equation

$$\left[\frac{1}{c^2}\frac{\partial^2}{\partial t^2} - \frac{\partial^2}{\partial r^2} - \frac{2}{r}\frac{\partial}{\partial r}\right]\phi_{00}(r,t) = 0 \tag{13}$$

For outgoing waves, general solutions of (13) take the form of a uniform spherical wave, i.e. $v_{nm}(r-ct)/r$. Using this result in (12) gives

$$\phi_{nm} = \prod_{j=1}^{n}\left(\frac{\partial}{\partial r} - \frac{j-1}{r}\right)\frac{v_{nm}(r-ct)}{r}, \quad n \geqslant 1,\ |m| \leqslant n \tag{14}$$

As shown in [8], expanding (14) leads to an operator form involving $n$th-order radial derivatives acting on $v_{nm}$. By induction, the $n$th term appearing in the operator takes the form

$$\phi_{nm}(r,t) = \sum_{j=0}^{n}\frac{(-1)^j}{r^{j+1}}a_n^j\frac{\partial^{n-j}}{\partial r^{n-j}}v_{nm}(r-ct) \tag{15}$$

with coefficients

$$a_n^j = \frac{(n+j)!}{2^j j!(n-j)!} \tag{16}$$

This result was first derived in (Lemma 7.1 [5]) using an alternate method involving an integral operator.

The expression for $\phi_{nm}$ given in (15) involves high-order radial derivatives which are difficult to implement in a numerical method. To arrive at an equivalent but more tractable form, the special property of the wave functions $v_{nm}(r-ct)$

$$(-1)^k\frac{\partial^k}{\partial r^k}v_{nm}(r-ct) = \frac{1}{c^k}\frac{\partial^k}{\partial t^k}v_{nm}(r-ct) \tag{17}$$

is used to replace the radial derivatives in (15) with time derivatives with the result:

$$\phi_{nm}(r,t) = (-1)^n\sum_{j=0}^{n}\frac{1}{c^{n-j}}\frac{a_n^j}{r^{j+1}}\frac{\partial^{n-j}}{\partial t^{n-j}}v_{nm}(r-ct) \tag{18}$$

As shown in [6], a sequence of equivalent exact non-reflecting boundary conditions can be obtained by applying the local differential operators derived by Bayliss and Turkel [2] which annihilate increasing numbers of radial terms in the multipole expansion of $\phi(\mathbf{x},t)$, to (18).

The simplest form of the non-reflecting boundary condition is to apply the local operator

$$B_1 := \left(\frac{\partial}{\partial r} + \frac{1}{c}\frac{\partial}{\partial t} + \frac{1}{r}\right) \tag{19}$$

to (18) with the result,

$$\begin{aligned} B_1(\phi_{nm}) &= \left(\frac{\partial}{\partial r} + \frac{1}{c}\frac{\partial}{\partial t} + \frac{1}{r}\right)\phi_{nm}(r,t) \\ &= \frac{(-1)^{n+1}}{r}\sum_{j=1}^{n}\frac{j}{c^{n-j}}\frac{a_n^j}{r^{j+1}}\frac{\partial^{n-j}}{\partial t^{n-j}}v_{nm}(r-ct) \end{aligned} \tag{20}$$

 

Multiplying (20) by $Y_{nm}(\theta,\varphi)$, summing over $n$ and $m$, setting $r=R$ and using (9) yields

$$B_1[\phi(R,\theta,\varphi,t)] = -\frac{1}{R}\sum_{n=1}^{\infty}\sum_{m=-n}^{n} Y_{nm}(\theta,\varphi)\sum_{j=1}^{n}\frac{j}{c^{n-j}}\frac{a_n^j}{R^j}\frac{\mathrm{d}^{n-j}}{\mathrm{d}t^{n-j}}w_{nm}(t) \tag{21}$$

where

$$w_{nm}(t) = (-1)^n v_{nm}(R-ct)/R \tag{22}$$

Equation (21) is the exact non-reflecting boundary condition given in [5], Theorem 7.1, with the functions $w_{nm}$ rescaled by $(-1)^n/R$. The local $B_1$ operator is exact for the breathing mode $\phi_{00} = v_n(r-ct)/r$ and annihilates the leading radial terms $1/r$ and $1/r^2$ for higher-order modes.

Similarly, an alternate form of non-reflecting boundary condition can be obtained by applying the second-order local operator of Bayliss and Turkel [2] to (18)

$$\begin{aligned} B_2(\phi_{nm}) &= \left(\frac{\partial}{\partial r}+\frac{1}{c}\frac{\partial}{\partial t}+\frac{3}{r}\right)\left(\frac{\partial}{\partial r}+\frac{1}{c}\frac{\partial}{\partial t}+\frac{1}{r}\right)\phi_{nm} \\ &= \frac{(-1)^n}{r}\sum_{j=2}^{n}\frac{j(j-1)}{c^{n-j}}\frac{a_n^j}{r^{j+2}}\frac{\partial^{n-j}}{\partial t^{n-j}}v_{nm}(r-ct) \end{aligned} \tag{23}$$

resulting in

$$B_2[\phi(R,\theta,\varphi,t)] = \frac{1}{R}\sum_{n=2}^{\infty}\sum_{m=-n}^{n} Y_{nm}(\theta,\varphi)\sum_{j=2}^{n}\frac{j(j-1)}{c^{n-j}}\frac{a_n^j}{R^{j+1}}\frac{\mathrm{d}^{n-j}}{\mathrm{d}t^{n-j}}w_{nm}(t) \tag{24}$$

We note that the term $j=1$ in the series (21) does not appear in (24). As a result, the local operator $B_2\phi$ is exact for the first two modes $n=0,1$ and annihilates the leading terms up to $1/r^4$ for higher-order modes.

The functions $w_{nm}(t)$ appearing in (21) and (24) are solutions to the ordinary differential equations of order $n$ obtained by evaluating (18) at $r=R$,

$$\frac{1}{c^n}\frac{\mathrm{d}^n}{\mathrm{d}t^n}w_{nm}(t) = -\sum_{j=1}^{n}\frac{1}{c^{n-j}}\frac{a_n^j}{R^j}\frac{\mathrm{d}^{n-j}}{\mathrm{d}t^{n-j}}w_{nm}(t) + \phi_{nm}(R,t) \tag{25}$$

with initial conditions,

$$w_{nm}(0) = \frac{\mathrm{d}}{\mathrm{d}t}w_{nm}(0) = \cdots = \frac{\mathrm{d}^{n-1}}{\mathrm{d}t^{n-1}}w_{nm}(0) = 0 \tag{26}$$

The $n$th-order differential equation (25) is reduced to a first-order system of differential equations by introducing function

$$z_{nm}^i(t) = \frac{1}{R^{i-1}c^{n-i}}\frac{a_n^i}{a_n^1}\frac{\mathrm{d}^{n-i}}{\mathrm{d}t^{n-i}}w_{nm}(t), \quad i=1,\ldots,n \tag{27}$$

The resulting system of equations can be written in standard matrix form as

$$\frac{\mathrm{d}}{\mathrm{d}t}\mathbf{z}_{nm}(t) = \mathbf{A}_n\mathbf{z}_{nm}(t) + \Phi_{nm}(t) \tag{28}$$

 

with coefficients

$$A_n^{ij} = \begin{cases} \frac{-n(n+1)c}{2R} & \text{if } i = 1 \\ \frac{(n+i)(n-i+1)c}{2iR} & \text{if } i = j+1 \\ 0 & \text{otherwise} \end{cases} \tag{29}$$

The non-homogeneous vector function $\Phi_{nm}$ has the $nm$-th coefficient of $\phi$ on $\Gamma$ as its only non-zero component

$$\Phi_{nm}(t) = [c\,\phi_{nm}|_{r=R}, 0, \ldots, 0]^{\mathrm{T}} \tag{30}$$

where

$$\phi_{nm}|_{r=R} = (\phi, Y_{nm})_\Gamma = \int_0^{2\pi} \int_0^{\pi} Y_{nm}^*(\theta, \varphi)\ \phi(R, \theta, \varphi, t) \sin\theta \,\mathrm{d}\theta \,\mathrm{d}\varphi \tag{31}$$

and the star indicates complex conjugate. The scaling used in (27) eliminates the large $a_n^j$ that appears in (21) and (24) and leads to a well-conditioned coefficient matrix $\mathbf{A}$. The alternate scaling used in [5, 6] leads to a system of differential equations in the same form as (28) but with a different coefficient matrix. The initial conditions $\mathbf{z}_{nm}(0) = 0$ follow directly from (26).

To eliminate the high-order derivatives appearing in (21), $w_{nm}$ and its derivatives are replaced with $\mathbf{z}_{nm}$, with the result,

$$B_1\phi = -\frac{1}{R} \sum_{n=1}^{\infty} \sum_{m=-n}^{n} (\mathbf{e}_n \cdot \mathbf{z}_{mn})\, Y_{nm}(\theta, \varphi) \quad \text{on } \Gamma \times ]0, T[ \tag{32}$$

where $\mathbf{e}_n = \{e_n^j\}$ and

$$e_n^j = n(n+1)j/2R, \quad j = 1, \ldots, n \tag{33}$$

Similarly, equation (24) can be written as

$$B_2\phi = \frac{1}{R} \sum_{n=2}^{\infty} \sum_{m=-n}^{n} (\tilde{\mathbf{e}}_n \cdot \mathbf{z}_{nm})\, Y_{nm}(\theta, \varphi) \quad \text{on } \Gamma \times ]0, T[ \tag{34}$$

where $\tilde{\mathbf{e}}_n = \{\tilde{e}_n^j\}$ and

$$\tilde{e}_n^j = n(n+1)j(j-1)/2R^2, \quad j = 1, \ldots, n \tag{35}$$

Result (34) has the same form as equation (5.21) in [6], but with a different scaling for $\tilde{\mathbf{e}}_n$.

The summation over the series in (32) and (34) may be viewed as an extension of the local $B_1$ and $B_2$ operators of Bayliss and Turkel [2], respectively. In computation, the sum over $n$ in (32) and (34) is truncated at a finite value $N \geqslant 1$, and $N \geqslant 2$, respectively. The modes $n \leqslant N$ will be represented exactly for both (32) and (34). For modes $\phi_{nm} = (\phi, Y_{nm})_\Gamma$, $n > N$, (32) reduces to $B_1\phi = 0$ on $\Gamma$, while (34) reduces to $B_2\phi = 0$ on $\Gamma$. The $B_1$ operator annihilates radial terms in the multipole expansion [15]:

$$\phi(r, \theta, \varphi, t) = \sum_{j=1}^{\infty} \frac{g_j(r - ct, \theta, \varphi)}{r^j} \tag{36}$$

 

with leading error term $B_1\phi = \mathcal{O}(1/r^3)$, while the $B_2$ operator has leading error term $B_2\phi = \mathcal{O}(1/r^5)$. Therefore, when truncated at a finite value $N$, boundary condition (34) is expected to approximate the modes $n > N$ with greater accuracy than (32), i.e., the truncated boundary condition (34) remains exact for the low modes $n \leqslant N$, but becomes more accurate than (32) for the high modes $n > N$.

## 3. FINITE ELEMENT FORMULATION

Implementation of (32) and (34) with an alternate scaling using finite difference methods is discussed in [6]. In [7, 8] we implemented (32) in a standard semidiscrete finite element formulation with several alternative implicit and explicit time-integrators. In this section we show how to implement (34) in the finite element method. Two alternative implementations of the (modified) boundary operators are proposed. In the first, the boundary operator is implemented directly as a 'natural' boundary condition in the variational equation. In the second, the operator is implemented indirectly by introducing auxiliary variables on the nonreflecting boundary $\Gamma$.

To use (34) in a finite element formulation, we reformulate the boundary condition and derive an equivalent but more tractable form, which does not involve high-order radial derivatives. For finite element implementation, second-order radial derivatives appearing in (34) are eliminated in favour of tangential derivatives on the boundary $\Gamma$, through use of the wave equation in spherical coordinates,

$$\frac{\partial^2\phi}{\partial r^2} = \frac{1}{c^2}\frac{\partial^2\phi}{\partial t^2} - \frac{2}{r}\frac{\partial\phi}{\partial r} - \frac{1}{r^2}\Delta_\Gamma\phi \tag{37}$$

where

$$\Delta_\Gamma\phi = \frac{1}{\sin\theta}\frac{\partial}{\partial\theta}\left(\sin\theta\frac{\partial\phi}{\partial\theta}\right) + \frac{1}{\sin^2\theta}\frac{\partial^2\phi}{\partial\varphi^2} \tag{38}$$

is the Laplace–Beltrami operator. Expanding the $B_2$ operator in (34) and eliminating the high-order radial derivative $\partial^2\phi/\partial r^2$ using (37), we obtain the alternative form of (34) given by

$$\begin{aligned}\frac{\partial\phi}{\partial r} + \frac{R}{c}\frac{\partial^2\phi}{\partial r\partial t} + \frac{R}{c^2}\frac{\partial^2\phi}{\partial t^2} + \frac{2}{c}\frac{\partial\phi}{\partial t} + \frac{1}{R}\phi - \frac{1}{2R}\Delta_\Gamma\phi \\ = \frac{1}{2}\sum_{n=2}^{\infty}\sum_{m=-n}^{n}(\tilde{\mathbf{e}}_n\cdot\mathbf{z}_{nm})Y_{nm} \quad \text{on } \Gamma\times]0,T[\end{aligned} \tag{39}$$

The variational equation within $\Omega$ is obtained as usual by multiplying the wave equation (5) with a weighting function $\delta\phi$, and using the divergence theorem to obtain,

$$\frac{1}{c^2}\left(\delta\phi, \frac{\partial^2\phi}{\partial t^2}\right)_\Omega + (\nabla\delta\phi, \nabla\phi)_\Omega = \left(\delta\phi, \frac{\partial\phi}{\partial n}\right)_\Gamma + (\delta\phi, f)_\Omega \tag{40}$$

where

$$(\delta\phi, \phi)_\Omega := \int_\Omega \delta\phi\,\phi\,\mathrm{d}\Omega$$

$$(\delta\phi, \phi)_\Gamma := \int_\Gamma \delta\phi\,\phi\,\mathrm{d}\Gamma$$

are standard inner products.

 

### 3.1. Direct implementation

For a spherical boundary, the normal derivative on $\Gamma$ is equivalent to a radial derivative, i.e. $\partial\phi/\partial n = \partial\phi/\partial r$. The exact non-reflecting boundary condition (39) may be implemented directly by replacing the normal derivative in (40) with the radial derivative in (39), with the result

$$\frac{1}{c^2}\left(\delta\phi, \frac{\partial^2\phi}{\partial t^2}\right)_\Omega + (\nabla\delta\phi, \nabla\phi)_\Omega + \frac{R}{c^2}\left(\delta\phi, \frac{\partial^2\phi}{\partial t^2}\right)_\Gamma + \frac{R}{c}\left(\delta\phi, \frac{\partial^2\phi}{\partial r\partial t}\right)_\Gamma + \frac{2}{c}\left(\delta\phi, \frac{\partial\phi}{\partial t}\right)_\Gamma + \frac{1}{R}(\delta\phi, \phi)_\Gamma + \frac{R}{2}(\nabla^{\mathrm{s}}\delta\phi, \nabla^{\mathrm{s}}\phi)_\Gamma = L(\delta\phi) \tag{41}$$

where

$$L(\delta\phi) = (\delta\phi, f)_\Omega + \frac{1}{2}\sum_{n=2}^{\infty}\sum_{m=-n}^{n}\tilde{\mathbf{e}}_n \cdot \mathbf{z}_{nm}\,(\delta\phi, Y_{nm})_\Gamma \tag{42}$$

In the above, $\nabla^{\mathrm{s}}$ denotes the surface gradient on a sphere,

$$\nabla^{\mathrm{s}}\phi = \frac{1}{R}\frac{\partial\phi}{\partial\theta}\hat{\mathbf{e}}_\theta + \frac{1}{R\sin\theta}\frac{\partial\phi}{\partial\varphi}\hat{\mathbf{e}}_\varphi \quad \text{on } \Gamma \tag{43}$$

where $\hat{\mathbf{e}}_\theta$, $\hat{\mathbf{e}}_\varphi$ are unit vectors in $\theta$ and $\varphi$ directions, respectively. In deriving (41), the following identity was used:

$$\frac{1}{2R}(\delta\phi, \Delta_\Gamma\phi)_\Gamma = -\frac{R}{2}(\nabla^{\mathrm{s}}\delta\phi, \nabla^{\mathrm{s}}\phi)_\Gamma \tag{44}$$

This boundary term is obtained by integration-by-parts on $\Gamma$ and the periodic condition $\delta\phi(R,\theta,0) = \delta\phi(R,\theta,2\pi)$.

The objective of the weak form of the initial boundary value problem with direct implementation of (39) is to find $\phi(\mathbf{x},t)$ in $\Omega\cup\Gamma$ such that the variational equation (41) is satisfied for all admissible weighting functions $\delta\phi$, and where $\mathbf{z}_{nm}(t)$ satisfies the system of first-order equations (28).

Using a standard Galerkin finite element approximation $\phi \approx \mathbf{N}(x)\phi(t)$, results in the following second-order system of ordinary differential equations in time for the global solution vector $\phi(t)$:

$$\mathbf{M}\ddot{\phi}(t) + \mathbf{C}\dot{\phi}(t) + \mathbf{K}\phi(t) = \mathbf{F}(t), \quad t>0 \tag{45}$$

with arrays:

$$\mathbf{M} = \int_\Omega \frac{1}{c^2}\mathbf{N}^T\mathbf{N}\,d\Omega + \int_\Gamma \frac{R}{c^2}\mathbf{N}^{\mathrm{T}}\mathbf{N}\,\mathrm{d}\Gamma \tag{46}$$

$$\mathbf{C} = \int_\Gamma \mathbf{N}^{\mathrm{T}}\left(\frac{2}{c}\mathbf{N} + \frac{R}{c}\frac{\partial\mathbf{N}}{\partial r}\right)\mathrm{d}\Gamma \tag{47}$$

$$\mathbf{K} = \int_\Omega (\nabla\mathbf{N})^{\mathrm{T}}(\nabla\mathbf{N})\,\mathrm{d}\Omega + \int_\Gamma \frac{1}{R}\mathbf{N}^{\mathrm{T}}\mathbf{N} + \frac{R}{2}(\nabla^{\mathrm{s}}\mathbf{N})^{\mathrm{T}}(\nabla^{\mathrm{s}}\mathbf{N})\,\mathrm{d}\Gamma \tag{48}$$

$$\mathbf{F}(t) = \int_\Omega \mathbf{N}^{\mathrm{T}} f(\mathbf{x},t)\,\mathrm{d}\Omega + \frac{1}{2}\sum_{n=2}^{N}\sum_{m=-n}^{n}\tilde{\mathbf{e}}_n \cdot \mathbf{z}_{nm}(t)\int_\Gamma \mathbf{N}^{\mathrm{T}}Y_{nm}\,\mathrm{d}\Gamma \tag{49}$$

and $\mathbf{N}(\mathbf{x})$ is a vector array of $C^\circ$ basis functions with compact support associated with each node in a finite element mesh. The sum over $n$ is truncated at a finite value $N$. For $N<2$, the

 

formulation reduces to the direct implementation of the local $B_2$ boundary condition described in [3]. For $N \geqslant 2$, the NRBC is global over $\Gamma$, yet only requires inner products of spherical harmonics within the force vector $\mathbf{F}$. As a result, the NRBC is easy to implement and does not disturb the banded/sparse structure of the finite element matrix equations. In (49), the functions $\mathbf{z}_{nm} = \{z_{nm}^j\}$ are solutions to the system of first-order equations (28).

### 3.2. Indirect implementation

The direct implementation of the exact NRBC (39) results in an unsymmetric damping matrix (47) which involves evaluation of a radial derivative on $\Gamma$. In order to obtain a symmetric system and to avoid inaccuracies caused by approximating the radial derivative, an indirect implementation is developed. This alternative formulation is based on the procedure used in [10] for the symmetrization of a second-order local absorbing boundary condition.

Recognizing the hierarchical structure inherent in the $B_2$ operator, equation (39) can be split in the form,

$$\frac{R}{c}\frac{\partial}{\partial t}(B_1\phi) + B_1\phi - \frac{1}{2R}\Delta_\Gamma\phi - \frac{1}{2}\sum_{n=2}^{\infty}\sum_{m=-n}^{n}(\tilde{\mathbf{e}}_n \cdot \mathbf{z}_{nm})\, Y_{nm} = 0 \tag{50}$$

By introducing auxiliary variables $\psi(\theta, \varphi, t)$ and $q_{nm}(t)$ on $\Gamma$ such that

$$\frac{1}{2R}\Delta_\Gamma\phi = \frac{R}{c}\frac{\partial}{\partial t}\frac{1}{2R}\Delta_\Gamma\psi + \frac{1}{2R}\Delta_\Gamma\ \psi, \quad \psi(\theta, \varphi, 0) = 0 \tag{51}$$

and

$$\tilde{\mathbf{e}}_n \cdot \mathbf{z}_{nm}(t) = \frac{R}{c}\frac{\mathrm{d}}{\mathrm{d}t}q_{nm}(t) + q_{nm}(t), \quad q_{mn}(0) = 0 \tag{52}$$

Equation (50) takes the form

$$\frac{R}{c}\frac{\partial}{\partial t}Q + Q = 0 \tag{53}$$

where

$$Q(\theta, \varphi, t) = B_1\phi - \frac{1}{2R}\Delta_\Gamma\psi - \frac{1}{2}\sum_{n=2}^{\infty}\sum_{m=-n}^{n} q_{nm} Y_{nm} \tag{54}$$

The general solution to (53) is

$$Q(\theta, \varphi, t) = \alpha(\theta, \varphi)\mathrm{e}^{-(c/R)t} \tag{55}$$

where the function $\alpha(\theta, \varphi)$ is determined by the initial conditions on $Q$. From (8), and assuming $\psi(\theta, \varphi, 0) = 0$ and $q_{nm}(0) = 0$, the solution satisfies the homogeneous initial condition,

$$Q(\theta, \varphi, 0) = 0 \tag{56}$$

Evaluating (55) at $t = 0$ and using (56), gives the solution $Q(\theta, \varphi, t) = 0$, for $0 < t < T$, or

$$\frac{\partial\phi}{\partial r} + \frac{1}{c}\frac{\partial\phi}{\partial t} + \frac{1}{R}\phi - \frac{1}{2R}\Delta_\Gamma\psi = \frac{1}{2}\sum_{n=2}^{\infty}\sum_{m=-n}^{n} q_{nm} Y_{nm} \quad \text{on } \Gamma\times]0, T[ \tag{57}$$

The system of equations (57), (51), and (52) define an alternative form of the exact NRBC (39).

 

The variational equation within $\Omega$ is obtained by replacing the normal derivative in (40) with the radial derivative appearing in (57), and integrating-by-parts on $\Gamma$, with the result,

$$\frac{1}{c^2}\left(\delta\phi, \frac{\partial^2\phi}{\partial t^2}\right)_\Omega + (\nabla\delta\phi, \nabla\phi)_\Omega + \frac{1}{c}\left(\delta\phi, \frac{\partial\phi}{\partial t}\right)_\Gamma + \frac{1}{R}(\delta\phi, \phi)_\Gamma + \frac{R}{2}(\nabla^s\delta\phi, \nabla^s\psi) = L(\delta\phi) \tag{58}$$

where

$$L(\delta\phi) = (\delta\phi, f)_\Omega + \frac{1}{2}\sum_{n=2}^{\infty}\sum_{m=-n}^{n} q_{nm}(t)(\delta\phi, Y_{nm})_\Gamma \tag{59}$$

Multiplying (51) with the weighting function $\delta\psi$, then integrating by parts, and combining with (58) leads to the variational equation,

$$\frac{1}{c^2}\left(\delta\phi, \frac{\partial^2\phi}{\partial t^2}\right)_\Omega + (\nabla\delta\phi, \nabla\phi)_\Omega + \frac{1}{c}\left(\delta\phi, \frac{\partial\phi}{\partial t}\right)_\Gamma + \frac{1}{R}(\delta\phi, \phi)_\Gamma + D(\delta\phi, \psi)_\Gamma + D(\delta\psi, \phi)_\Gamma - \frac{R}{c}D\left(\delta\psi, \frac{\partial\psi}{\partial t}\right)_\Gamma - D(\delta\psi, \psi)_\Gamma = L(\delta\phi) \tag{60}$$

where the bilinear operator $D$ is defined as

$$D(\delta\psi, \psi)_\Gamma := \frac{R}{2}(\nabla^s\delta\psi, \nabla^s\psi)_\Gamma \tag{61}$$

The objective of the weak form of the initial boundary value problem with indirect implementation of the NRBC is to find $\phi(\mathbf{x}, t)$ in $\Omega \cup \Gamma$, and $\psi(\mathbf{x}, t)$ on $\Gamma$, such that the variational equation (60) is satisfied for all admissible weighting functions $\delta\phi$, and $\delta\psi$, and where $q_{nm}(t)$ and $\mathbf{z}_{nm}(t)$ satisfy the first-order equations (52) and (28), respectively.

Use of independent finite element approximations

$$\phi(\mathbf{x}, t) \approx \mathbf{N}_\phi(\mathbf{x})\phi(t) \quad \text{in } \Omega \cup \Gamma \tag{62}$$

$$\psi(\mathbf{x}, t) \approx \mathbf{N}_\psi(\mathbf{x})\psi(t) \quad \text{on } \Gamma \tag{63}$$

results in the symmetric system of matrix equations

$$\begin{bmatrix} \mathbf{M}_{\phi\phi} & \mathbf{0} \\ \mathbf{0} & \mathbf{0} \end{bmatrix} \begin{Bmatrix} \ddot{\phi}(t) \\ \ddot{\psi}(t) \end{Bmatrix} + \begin{bmatrix} \mathbf{C}_{\phi\phi} & \mathbf{0} \\ \mathbf{0} & \mathbf{C}_{\psi\psi} \end{bmatrix} \begin{Bmatrix} \dot{\phi}(t) \\ \dot{\psi}(t) \end{Bmatrix} + \begin{bmatrix} \mathbf{K}_{\phi\phi} & \mathbf{K}_{\phi\psi} \\ \mathbf{K}_{\psi\phi} & \mathbf{K}_{\psi\psi} \end{bmatrix} \begin{Bmatrix} \phi(t) \\ \psi(t) \end{Bmatrix} = \begin{Bmatrix} \mathbf{F}(t) \\ \mathbf{0} \end{Bmatrix} \tag{64}$$

where

$$\mathbf{M}_{\phi\phi} = \int_\Omega \frac{1}{c^2}\mathbf{N}_\phi^{\mathrm{T}} N_\phi \, \mathrm{d}\Omega \tag{65}$$

$$\mathbf{C}_{\phi\phi} = \int_\Gamma \frac{1}{c}\mathbf{N}_\phi^{\mathrm{T}} N_\phi \, \mathrm{d}\Gamma, \quad \mathbf{C}_{\psi\psi} = \int_\Gamma -\frac{R^2}{2c}(\nabla^s\mathbf{N}_\psi)^{\mathrm{T}}(\nabla^s\mathbf{N}_\psi)\, \mathrm{d}\Gamma \tag{66}$$

$$\mathbf{K}_{\phi\phi} = \int_\Omega (\nabla\mathbf{N}_\phi)^{\mathrm{T}}(\nabla\mathbf{N}_\phi)\, \mathrm{d}\Omega + \int_\Gamma \frac{1}{R}\mathbf{N}_\phi^{\mathrm{T}}\mathbf{N}_\phi \, \mathrm{d}\Gamma \tag{67}$$

 

$$\mathbf{K}_{\phi\psi} = \int_\Gamma \frac{R}{2} (\nabla^s \mathbf{N}_\phi)^T (\nabla^s \mathbf{N}_\psi)\, d\Gamma, \quad \mathbf{K}_{\psi\phi} = \mathbf{K}_{\phi\psi}^T \tag{68}$$

$$\mathbf{K}_{\psi\psi} = \int_\Gamma -\frac{R}{2} (\nabla^s \mathbf{N}_\psi)^T (\nabla^s \mathbf{N}_\psi)\, d\Gamma \tag{69}$$

$$\mathbf{F}(t) = \int_\Omega \mathbf{N}_\phi^T f(\mathbf{x}, t)\, d\Omega + \frac{1}{2} \sum_{n=2}^{N} \sum_{m=-n}^{n} q_{nm}(t) \int_\Gamma \mathbf{N}_\phi^T Y_{nm}\, d\Gamma \tag{70}$$

In the above, $\mathbf{N}_\phi \in C^0$ and $\mathbf{N}_\psi \in C^0$ are standard arrays of basis functions with compact support associated with each node in the finite element mesh in $\Omega \cup \Gamma$, and on the boundary $\Gamma$, respectively.

From the expression for the mass, damping, and stiffness matrices, we note that the indirect implementation of the non-reflecting boundary condition leads to a symmetric system of matrix equations, and avoids the unsymmetric damping matrix present in the direct implementation, albeit at the expense of solving for the additional unknowns $\psi(t)$ on the truncating boundary $\Gamma$.

We further note that the auxiliary function $\psi$ does not explicitly appear in the variational equation (60); instead only its surface gradient $\nabla^s \psi$ is present. As a result, a family of solutions for $\psi$ that differ by a constant will satisfy (60). At the discrete level, this will result in a solution matrix that is rank deficient by one. To obtain a unique solution, the function $\psi$ may be constrained at one arbitrary node on the truncation boundary. The value used to constrain the auxiliary function $\psi$ at that node is inconsequential to the unique solution for $\phi$, and may be set to zero.

*3.2.1. Specialization to axisymmetric case.* For axisymmetric problems, the functions $\phi(r, \theta, t)$ and $\psi(\theta, t)$ are independent of the circumferential coordinate $\varphi$, so that the surface gradient reduces to,

$$\nabla^s \phi = \frac{1}{R} \frac{\partial \phi}{\partial \theta} \hat{\mathbf{e}}_\theta \quad \text{on } \Gamma \tag{71}$$

and the bilinear operator $D$ defined in (61), and appearing in the variational equation (60), specializes to

$$D(\delta\psi, \psi)_\Gamma = \frac{1}{2R} (\delta\psi_{,\theta}, \psi_{,\theta})_\Gamma \tag{72}$$

In the above, the comma indicates a derivative.

In this case, only the function $\psi_{,\theta}$ is present in the variational equation. Therefore, another approach to obtain a unique solution, which is successfully used in solving the axisymmetric problems in this paper, is to directly approximate the function $\chi = \psi_{,\theta}$ instead of $\psi$ itself. Introducing a standard FE approximation $\chi(\mathbf{x}, t) \approx \mathbf{N}_\chi(\mathbf{x}) \chi(\mathbf{t})$ on $\Gamma$ into the variational equation leads to the matrix system,

$$\begin{bmatrix} \mathbf{M}_{\phi\phi} & \mathbf{0} \\ \mathbf{0} & \mathbf{0} \end{bmatrix} \begin{Bmatrix} \ddot{\phi}(t) \\ \ddot{\chi}(t) \end{Bmatrix} + \begin{bmatrix} \mathbf{C}_{\phi\phi} & \mathbf{0} \\ \mathbf{0} & \mathbf{C}_{\chi\chi} \end{bmatrix} \begin{Bmatrix} \dot{\phi}(t) \\ \dot{\chi}(t) \end{Bmatrix} + \begin{bmatrix} \mathbf{K}_{\phi\phi} & \mathbf{K}_{\phi\chi} \\ \mathbf{K}_{\chi\phi} & \mathbf{K}_{\chi\chi} \end{bmatrix} \begin{Bmatrix} \phi(t) \\ \chi(t) \end{Bmatrix} = \begin{Bmatrix} \mathbf{F}(t) \\ \mathbf{0} \end{Bmatrix} \tag{73}$$

 

where

$$\mathbf{C}_{\chi\chi} = \int_{\Gamma} -\frac{1}{2c}\mathbf{N}_{\chi}^{\mathrm{T}}\,\mathbf{N}_{\chi}\,\mathrm{d}\Gamma \tag{74}$$

$$\mathbf{K}_{\phi\chi} = \int_{\Gamma} \frac{1}{2R}\mathbf{N}_{\phi,\theta}^{\mathrm{T}}\,\mathbf{N}_{\chi}\,\mathrm{d}\Gamma, \quad \mathbf{K}_{\chi\phi} = \mathbf{K}_{\phi\chi}^{\mathrm{T}} \tag{75}$$

$$\mathbf{K}_{\chi\chi} = \int_{\Gamma} -\frac{1}{2R}\mathbf{N}_{\chi}^{\mathrm{T}}\,\mathbf{N}_{\chi}\,\mathrm{d}\Gamma \tag{76}$$

## 4. TIME INTEGRATION

Several time-marching schemes have been developed in [8] to integrate the semidiscrete equations (45) concurrently with the first-order equations (28) for the $B_1$ form of the non-reflecting boundary condition given in (32). The same schemes also apply to the direct implementation of the $B_2$ form of the non-reflecting boundary condition given in (39). However, for the indirect implementation of the NRBC, the time marching schemes given in [8] need to be modified to incorporate the solution of (52) together with (64) and (28).

In the first scheme for the indirect method, we adopt the Newmark family [11] to integrate (64). Let

$$\mathbf{d}^k = \{\phi(t_k), \psi(t_k)\}^{\mathrm{T}}$$
$$\mathbf{v}^k = \{\dot{\phi}(t_k), \dot{\psi}(t_k)\}^{\mathrm{T}}$$
$$\mathbf{a}^k = \{\ddot{\phi}(t_k), \ddot{\psi}(t_k)\}^{\mathrm{T}}$$

be the numerical solution and $\mathbf{F}^k = \{\mathbf{F}(t_k), \mathbf{0}\}^{\mathrm{T}}$ the force at time step $t_k = k\,\Delta t$, then the Newmark method in predictor/corrector form applied to (64) can be written as [12]:

*predictors*:

$$\tilde{\mathbf{d}}^{k+1} = \mathbf{d}^k + \Delta t\,\mathbf{v}^k + \frac{\Delta t^2}{2}(1-2\beta)\mathbf{a}^k \tag{77}$$

$$\tilde{\mathbf{v}}^{k+1} = \mathbf{v}^k + (1-\gamma)\Delta t a^k \tag{78}$$

*solve for* $\mathbf{a}^{k+1}$:

$$(\mathbf{M} + \gamma\Delta t\,\mathbf{C} + \beta\Delta t^2\mathbf{K})\mathbf{a}^{k+1} = \mathbf{F}^{k+1} - \mathbf{C}\tilde{\mathbf{v}}^{k+1} - \mathbf{K}\tilde{\mathbf{d}}^{k+1} \tag{79}$$

*correctors*:

$$\mathbf{d}^{k+1} = \tilde{\mathbf{d}}^{k+1} + \beta\Delta t^2\mathbf{a}^{k+1} \tag{80}$$

$$\mathbf{v}^{k+1} = \tilde{\mathbf{v}}^{k+1} + \gamma\Delta t\mathbf{a}^{k+1} \tag{81}$$

where

$$\mathbf{M} = \begin{bmatrix} \mathbf{M}_{\phi\phi} & \mathbf{0} \\ \mathbf{0} & \mathbf{0} \end{bmatrix}, \quad \mathbf{C} = \begin{bmatrix} \mathbf{C}_{\phi\phi} & \mathbf{0} \\ \mathbf{0} & \mathbf{C}_{\psi\psi} \end{bmatrix}, \quad \mathbf{K} = \begin{bmatrix} \mathbf{K}_{\phi\phi} & \mathbf{K}_{\phi\psi} \\ \mathbf{K}_{\psi\phi} & \mathbf{K}_{\psi\psi} \end{bmatrix} \tag{82}$$

Any of the members of the Newmark family may be used, including the second-order accurate $\gamma = \frac{1}{2}$, and unconditionally stable trapezoidal rule ($\beta = \frac{1}{4}$), and conditionally stable central difference method ($\beta = 0$).

 

The solution of (79) requires that the forcing term $\mathbf{F}^{k+1}$ be available at time step $t_{k+1}$, i.e.,

$$\mathbf{F}^{k+1} = \int_{\Omega} \mathbf{N}^{\mathrm{T}} f(\mathbf{x}, t_{k+1})\, \mathrm{d}\Omega - \frac{1}{R} \sum_{n=2}^{N} \sum_{m=-n}^{n} q_{nm}(t_{k+1}) \int_{\Gamma} \mathbf{N}^{\mathrm{T}} Y_{nm}\, \mathrm{d}\Gamma \tag{83}$$

To compute $\mathbf{a}^{k+1}$, we need the values of $q_{nm}(t)$ at $t = t_{k+1}$. The numerical solution $q_{nm}^{k+1} = q_{nm}(t_{k+1})$ to the first-order equation (52) is computed using the second-order Adams–Moulton method (trapezoidal rule):

$$\left(1 + \frac{c\Delta t}{2R}\right) q_{nm}^{k+1} = \left(1 - \frac{c\Delta t}{2R}\right) q_{nm}^{k} + \frac{c\Delta t}{2R} \left(\tilde{\mathbf{e}}_n \cdot \mathbf{z}_{nm}^{k} + \tilde{\mathbf{e}}_n \cdot \mathbf{z}_{nm}^{k+1}\right) \tag{84}$$

The numerical solution $\mathbf{z}_{nm}^{k+1} = \mathbf{z}_{nm}(t_{k+1})$ to the first-order differential equation (28) is computed concurrently using an explicit time-integrator; e.g. the second-order accurate Adams–Bashforth algorithm [13]:

$$\mathbf{z}_{nm}^{k+1} = \mathbf{z}_{nm}^{k} + \frac{\Delta t}{2}[3(\mathbf{A}_n \mathbf{z}_{nm}^{k} + \Phi_{nm}^{k}) - (\mathbf{A}_n \mathbf{z}_{nm}^{k-1} + \Phi_{nm}^{k-1})] \tag{85}$$

Note that (85) requires only the evaluation at $t = t_k$, the value at $t = t_{k-1}$ being known from the previous step. The stability condition imposed on $\Delta t$ by the explicit Adams–Bashforth method depends on the eigenvalues $\lambda$ of the coefficient matrix $\mathbf{A}_n$. The critical time step is,

$$\Delta t < \Delta t_{\mathrm{c}} = \frac{1}{\min(Re\, \lambda)} \tag{86}$$

As shown in [8], the critical time step $\Delta t_{\mathrm{c}}$ decreases when more terms $N$ are included in the non-reflecting boundary condition.

In the above method, an explicit algorithm is used first to compute $\mathbf{z}_{nm}^{k+1}$. This solution is then used to solve for $q_{nm}^{k+1}$ so that $\mathbf{F}^{k+1}$ is available to compute $\mathbf{d}^{k+1}$ from (79) and (80).

The complete algorithm is summarized as follows:

1. Set $q_{nm}^{0} = 0$, $\mathbf{z}_{nm}^{0} = \mathbf{z}_{nm}^{-1} = 0$, and initialize $\mathbf{d}^{0}$ and $\mathbf{v}^{0}$,
2. Calculate $\mathbf{a}^{0}$ from $\mathbf{M}\mathbf{a}^{0} = \tilde{\mathbf{F}}^{0} - \mathbf{C}\mathbf{v}^{0} - \mathbf{K}\mathbf{d}^{0}$, $\mathbf{d}^{-1} = \mathbf{d}^{0} - \Delta t \mathbf{v}^{0} + \dfrac{\Delta t^2}{2}\mathbf{a}^{0}$
3. Compute $\Phi_{nm}^{k}$ and $\Phi_{nm}^{k-1}$ from (31);
4. Compute $\mathbf{z}_{nm}^{k+1}$ using (85);
5. Compute $q_{nm}^{k+1}$ from (84);
6. Predict $\tilde{\mathbf{d}}^{k+1}$ and $\tilde{\mathbf{v}}^{k+1}$ from (77) and (78); Calculate $\mathbf{a}^{k+1}$ from (79); Update $\mathbf{d}^{k+1}$ and $\mathbf{v}^{k+1}$ using (80) and (81);
7. Increment $k$ to $k+1$, Go back to step 3.

Alternatively, $q_{nm}^{k+1}$ may be obtained directly from the explicit Adam–Bashforth method,

$$\mathbf{q}_{nm}^{k+1} = \mathbf{q}_{nm}^{k} + \frac{\Delta t}{2}\left[3\left(\frac{c}{R}\tilde{\mathbf{e}} \cdot \mathbf{z}_{nm}^{k} - \frac{c}{R} q_{nm}^{k}\right) - \left(\frac{c}{R}\tilde{\mathbf{e}} \cdot \mathbf{z}_{nm}^{k-1} - \frac{c}{R} q_{nm}^{k-1}\right)\right] \tag{87}$$

In this case, (28) may be solved using either the explicit Adams–Bashforth method (85), or with the implicit Adams–Moulton method, i.e.,

$$\left(\mathbf{I} - \frac{\Delta t}{2}\mathbf{A}_n\right) \mathbf{z}_{nm}^{k+1} = \left(\mathbf{I} + \frac{\Delta t}{2}\mathbf{A}_n\right) \mathbf{z}_{nm}^{k} + \frac{\Delta t}{2}(\Phi_{nm}^{k+1} + \Phi_{nm}^{k}) \tag{88}$$

 

Another approach is to apply the central difference method [14] directly to (64):

$$\left(\frac{1}{\Delta t^2}\mathbf{M}+\frac{1}{2\Delta t}\mathbf{C}\right)\mathbf{d}^{k+1}=\mathbf{F}^k-\mathbf{K}\mathbf{d}^k+\frac{1}{\Delta t^2}\mathbf{M}(2\mathbf{d}^k-\mathbf{d}^{k-1})+\frac{1}{2\Delta t}\mathbf{C}\mathbf{d}^{k-1} \tag{89}$$

The solution of (89) requires only that the forcing term $\mathbf{F}^k$ be available. Therefore, to compute $\mathbf{d}^{k+1}$, we only need to evaluate values of $q_{nm}(t)$ at $t=t_k$. In this case, both $q_{nm}^{k+1}$ and $\mathbf{z}_{nm}^{k+1}$ may be computed using the implicit second-order Adams–Moulton method.

## 5. NUMERICAL STUDIES

Numerical experiments are performed to assess the accuracy and convergence properties of the finite element implementation of the NRBC (39), using either the direct or indirect formulations discussed earlier. Comparisons are also made to the finite element solutions using the NRBC (32) and the first-order and second-order local boundary conditions $B_1$ and $B_2$ given in (1) and (2), respectively. We denote the NRBC (32) and (39) by NR1($N$) and NR2($N$), respectively, where $N$ defines the number of harmonics included in the truncated series. NR1(0) reduces to the local spherical damper $B_1$ defined in (1) and annihilates the first harmonic for outgoing waves; i.e., $B_1$ = NR1(0) is exact for the 'breathing' mode corresponding to $n=0$ in (9), yet only approximates higher modes. NR2(0) and NR2(1) reduces to the second-order local boundary condition $B_2$, and annihilates the first and second harmonics in (9).

For the purposes of this study, the conditionally stable implicit time integrator is used to advance the solution of the semidiscrete equations of motion as described in the previous section. For the direct implementation, an explicit algorithm is used first to compute $\mathbf{z}_{nm}^{k+1}$, so that $\mathbf{F}^{k+1}$ is available to compute $\mathbf{d}^{k+1}$ using a predictor/corrector form of the Newmark method specialized to the trapezoidal rule. For the indirect formulation, time integration is performed using an explicit solution for $\mathbf{z}_{nm}^{k+1}$ which is then used to solve for $q_{nm}^{k+1}$ so that $\mathbf{F}^{k+1}$ is available to compute $\mathbf{d}^{k+1}$ using the predictor/corrector form of the trapezoidal rule.

To study the accuracy of the non-reflecting boundary conditions for a problem involving an infinite number of spherical harmonics, we consider axisymmetric radiation from a circular piston on a sphere with radius $a=0.5$. The piston is represented by,

$$\begin{aligned}\phi(a,\theta,t)&=\sin\omega t \text{ for } 0^\circ\leqslant\theta\leqslant 15^\circ\\&=(30^\circ-\theta)\sin\omega t/15^\circ \quad \text{for } 15^\circ\leqslant\theta\leqslant 30^\circ\\&=0 \qquad\qquad\qquad\qquad \text{otherwise}\end{aligned}$$

This problem is challenging because the waves radiated at the piston pole $\theta=0^\circ$ are attenuated as they travel along longitudes down to the south pole $\theta=180^\circ$. In the region opposite the piston, the amplitude of the waves are significantly lower than near the piston, [16].

The problem is axisymmetric and independent of $\varphi$. Therefore it is sufficient to compute the solution in the domain $\Omega$ defined by the $(r,\theta)$ plane for $a\leqslant r\leqslant R$, and $0\leqslant\theta\leqslant\pi$. The computational domain is discretized with uniform meshes of standard 4-node bilinear axisymmetric finite elements.

### 5.1. Comparison of direct vs. indirect implementation

We begin with a calculation driven with a normalized frequency $\omega a/c=\pi$ on a mesh with $20\times 120$ elements and a truncation boundary at $R=1{\cdot}0$, (20 evenly spaced elements in $0{\cdot}5\leqslant r\leqslant$

 

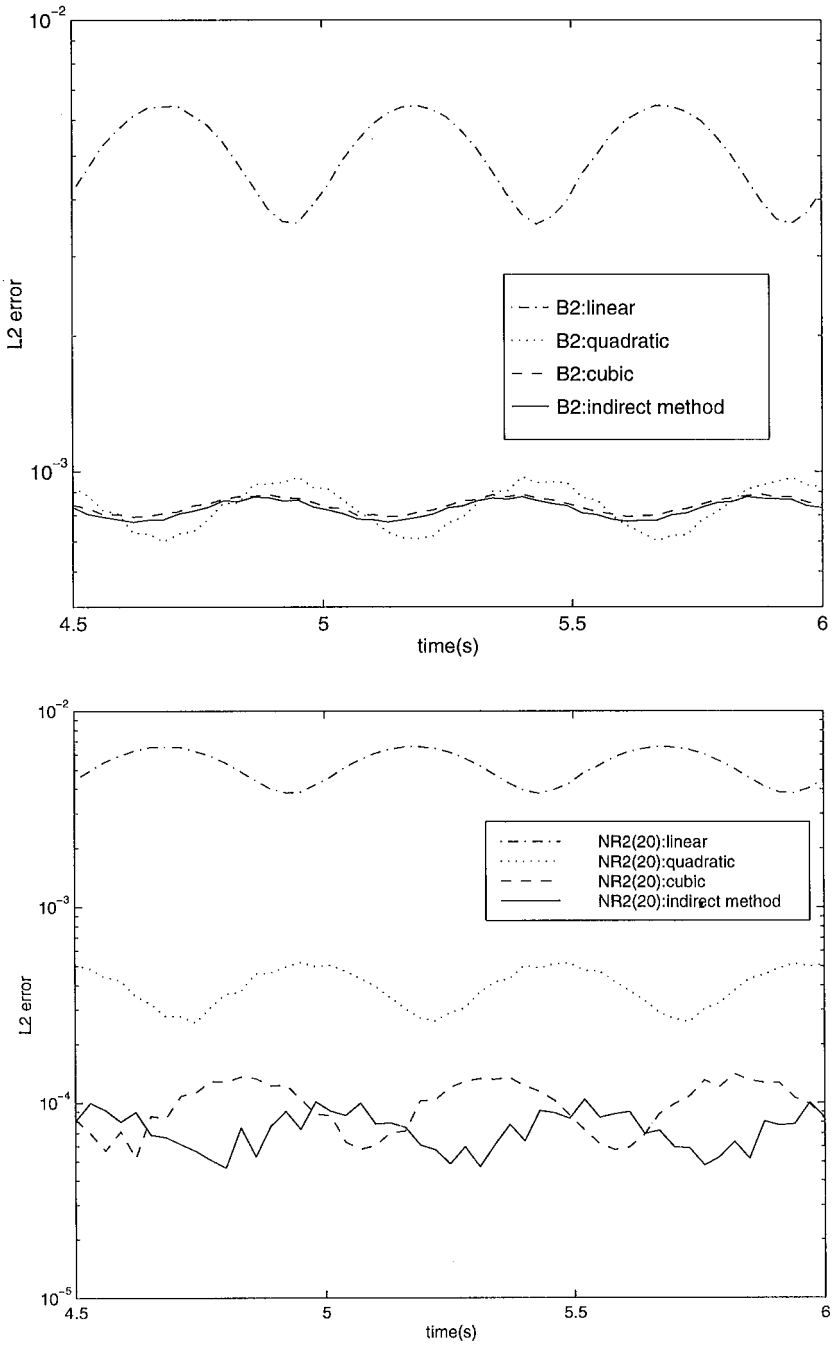


Figure 1. Instantaneous error $E(t)$ located at $r = 0{\cdot}75$ due to a radiating piston with normalized frequency $\omega a/c = \pi$ and truncation boundary radius $R/a = 2$. (Top) Results compared for direct and indirect implementation of local boundary condition $B_2$ (Bottom) Results compared for direct and indirect implementation of boundary condition NR2(20)

 

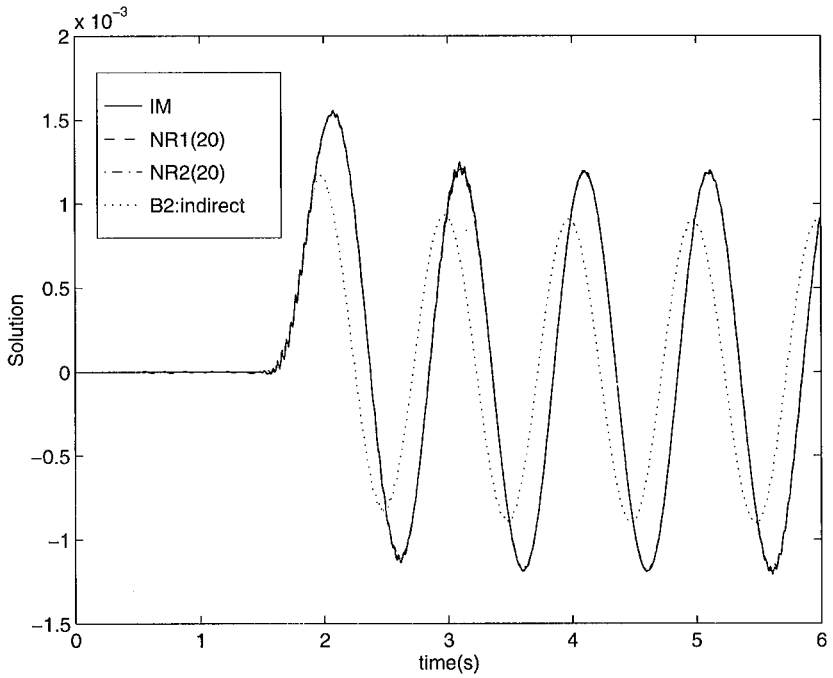


Figure 2. Time-histories for solution located at $r = 0{\cdot}75$, and $\theta = 180^\circ$ due to a radiating piston with normalized frequency $\omega a/c = \pi$ and truncation boundary radius $R/a = 1{\cdot}75$. Time-dependent solutions computed for B2, and NR1(20), NR2(20) compared to infinite mesh (IM) solution. High-frequency oscillations appearing in IM solution result from relatively course mesh in the far-field

$1{\cdot}0$, and 120 evenly spaced elements in $0 \leqslant \theta \leqslant \pi$). A time-harmonic solution is obtained by starting from rest with initial data $\phi_0$ and $\dot{\phi}_0$ equal to zero and driving the solution to steady state with a time step $\Delta t = 0{\cdot}005$. For a spherical truncation boundary set at $R = 1{\cdot}0$ and $N \leqslant 20$, the minimum eigenvalue (real part) of the system matrix $\mathbf{A}_n$ is $\lambda_{\min} = -13{\cdot}57$. For the Adams–Bashforth algorithm, this results in a stability condition $\Delta t < 0{\cdot}074$.

Solutions are compared using the direct vs. indirect implementation of NR2($N$). Results are also compared with a finite element solution obtained from a large mesh which extends beyond the region influenced by the transient disturbance, denoted IM. The direct formulation of NR2($N$) given in (41) requires evaluation of a radial derivative on $\Gamma$, resulting in a non-symmetric damping matrix (47). Using standard linear basis functions in the radial direction results in a constant approximation for the radial derivative, which introduces inaccuracies in the finite element solution. In order to overcome this difficulty, higher-order interpolation functions may be used in the radial direction for a layer of elements adjacent to the boundary.

Figure 1 shows the instantaneous error on a sphere $\Gamma_\rho$ located at radius $\rho = 0{\cdot}75$ and over the steady-state time interval $4{\cdot}5 < t < 6$. The instantaneous error $e(t) = \phi^h(t) - \phi^{\mathrm{h}}_\infty(t)$, measured in $L_2$ norm on a sphere $\Gamma_\rho$ is defined as,

$$E(t) = \left\{ \int_{\Gamma_\rho} \left[ \phi^{\mathrm{h}}(\rho, \theta, t) - \phi^{\mathrm{h}}_\infty(\rho, \theta, t) \right]^2 \, \mathrm{d}\Gamma \right\}^{1/2} \tag{90}$$

 

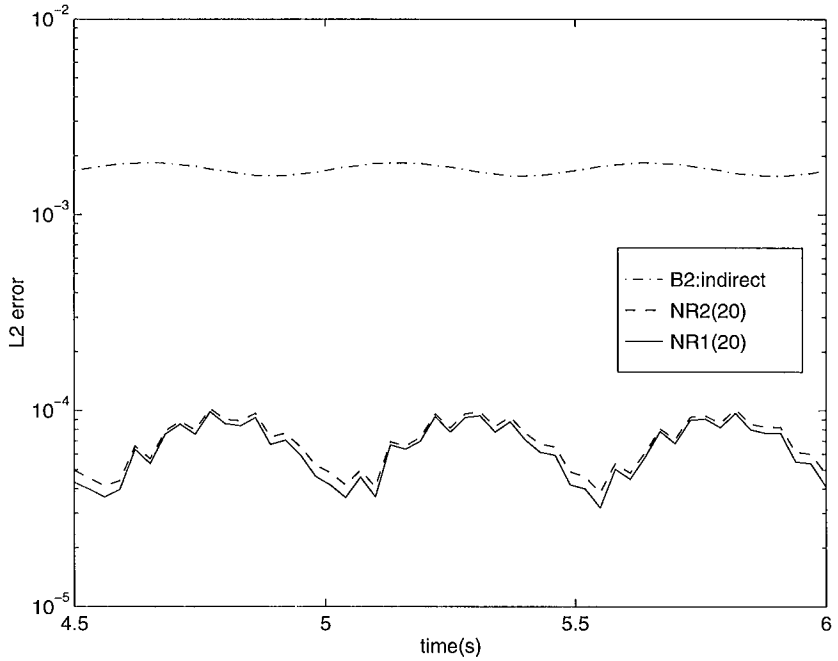


Figure 3. Instantaneous error $E(t)$ on the sphere $r = 0{\cdot}75$ due to a radiating piston with normalized frequency $\omega a/c = \pi$ and truncation boundary radius $R/a = 1{\cdot}75$. Results compared for boundary condition B2, NR1(20) and NR2(20). The error for B1 is approximately $10^{-2}$

where $\phi^{\mathrm{h}}$ is the finite element solution with non-reflecting boundary and $\phi^{\mathrm{h}}_{\infty}$ denotes the large mesh solution IM. For the solution $\phi^{\mathrm{h}}_{\infty}$, the mesh is extended to a larger domain with the same grid spacing used for $\phi^{\mathrm{h}}$. The magnitude of the absolute error $E(t)$ can be scaled by any constant, and will only serve as a means to compare the relative accuracy of the different boundary conditions.

In Figure 1(top) the numerical solutions obtained using a direct implementation of the local boundary condition $B_2$ is given where the radial derivative term appearing in the damping matrix is approximated using linear, quadratic and cubic interpolations for $\phi^{\mathrm{h}}$, evaluated on $\Gamma$. Results for the local $B_2$ operator implemented indirectly are shown for comparison. The results show a relatively large error when using linear interpolation to approximate the radial derivative in the direct formulation. When the interpolation is increased to quadratic, the error is reduced by nearly an order of magnitude. When the interpolation is increased to cubic, the accuracy of the direct formulation is approximately the same as the solution using the indirect implementation.

In Figure 1 (bottom), we perform the same comparison with the non-reflecting boundary condition NR2($N$) with $N = 20$. When a linear interpolation is used to approximate the radial derivative in the direct formulation of NR2(20), the error is nearly the same as that for the local $B_2$ condition with linear interpolation. This result indicates that the inaccuracies caused by the poor approximation of the radial derivative drives the error, regardless of how many terms $N$ are used in the series NR2($N$). When the radial interpolation is increased to quadratic, the error is reduced, but is still not optimal for $N = 20$. Only after the interpolation is increased to cubic does the error approach the high accuracy of the indirect formulation of NR2(20).

 

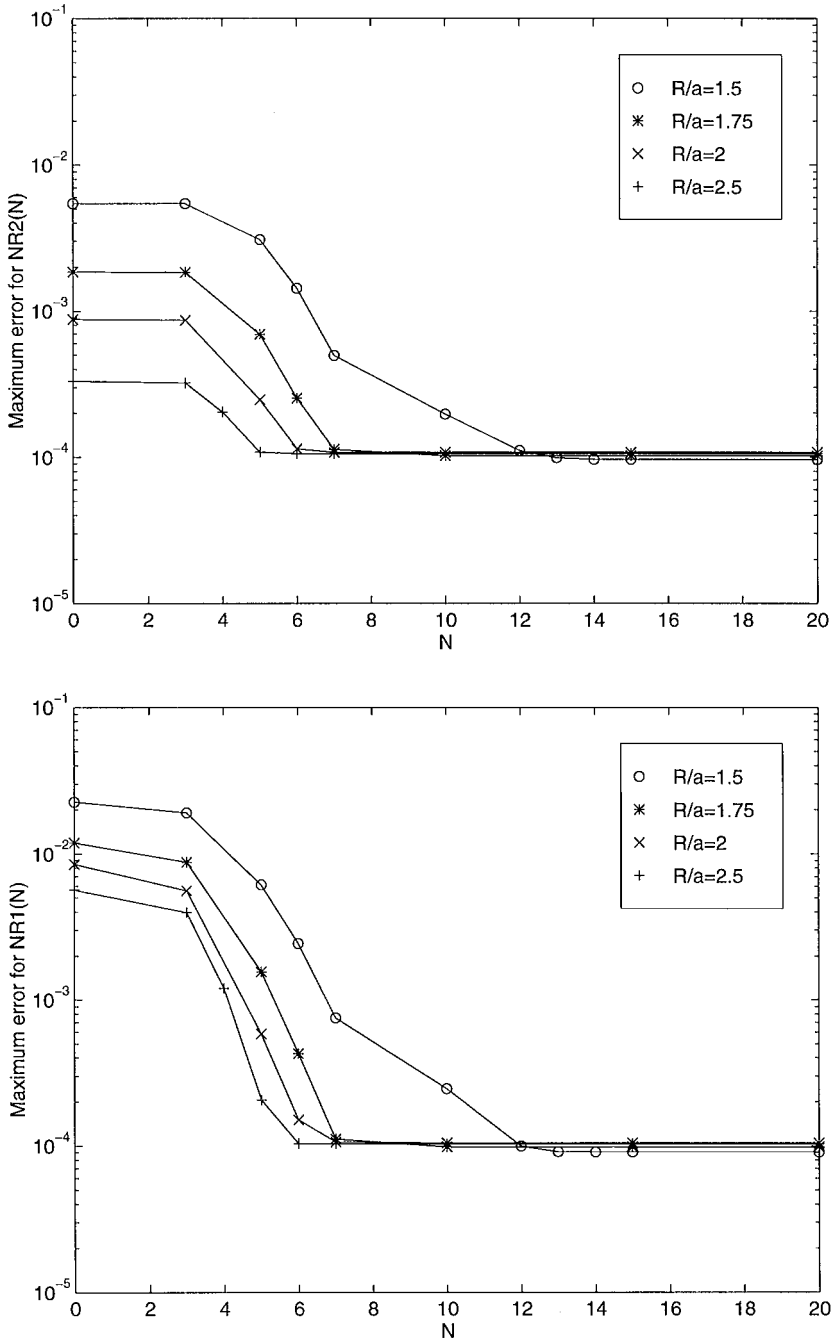


Figure 4. Maximum error measured at $r = 0{\cdot}75$ for the artificial boundary $\Gamma$ positioned at $R = 0{\cdot}75$ to $R = 1{\cdot}25$ and normalized frequency $\omega a/c = \pi$. (Top) NR2($N$) solution as a function of the number of terms $N$ included in the non-reflecting boundary condition. (Bottom) NR1($N$) solution as a function of the number of terms $N$ included in the non-reflecting boundary condition

 

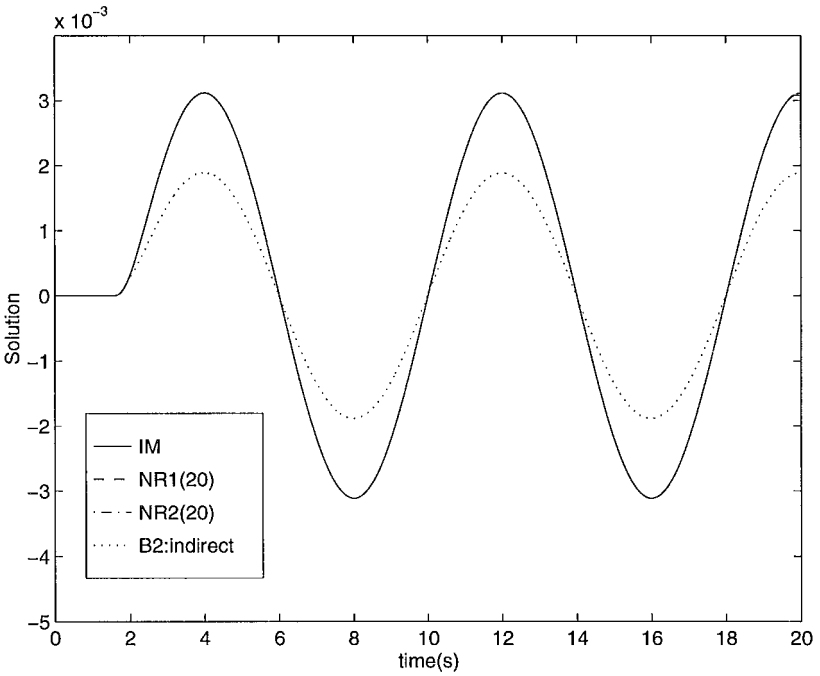


Figure 5. Time-histories at $r = 0{\cdot}75$ and $\theta = 180°$ and normalized frequency $\omega a/c = \pi/8$. Truncation boundary radius $R/a = 1{\cdot}75$. Results compared for boundary condition $B_2$, NR1(20) and NR2(20) with a truncation boundary radius $R/a = 1{\cdot}5$

These results demonstrate the disadvantage of the direct formulation for NR2($N$) caused by the difficulty in accurately approximating the radial derivative on the truncation boundary, and the resulting unsymmetric damping matrix. The indirect formulation using standard linear $C^0$ interpolation of NR2($N$) results in a symmetric system and accurate solutions. Therefore in the following numerical studies, we use the indirect implementation for NR2($N$).

### 5.2. *Comparison of NR1 and NR2*

Next, we compare the solutions computed using the boundary conditions NR1($N$) and NR2($N$). The computations are performed with a time step of $\Delta t = 0{\cdot}005$ and the truncation boundary set at $R = 0{\cdot}875$ resulting in $R/a = 1{\cdot}75$ and with the element size and frequency unchanged from the previous study, i.e. the calculation is driven with a normalized frequency $\omega a/c = \pi$ on a mesh with $15 \times 120$ elements.

Figure 2 shows time-dependent solutions at $\rho = 0{\cdot}75$, $\theta = 180°$, obtained using $B_2$, NR1(20), NR2(20) and the infinite mesh solution IM. The numerical solution using $B_2$ exhibits both large amplitude and phase errors. The solution obtained using NR1(20) and NR2(20) can barely be distinguished from the IM solution. The error $E(t)$ after the solution has reached steady state is shown in Figure 3. The error using the non-reflecting boundary conditions NR1($N$) and NR2($N$) with $N = 20$ is reduced by an order of magnitude compared to the local $B_2$ boundary condition. The error using the local $B_1$ operator is significantly higher with an average value of approximately

 

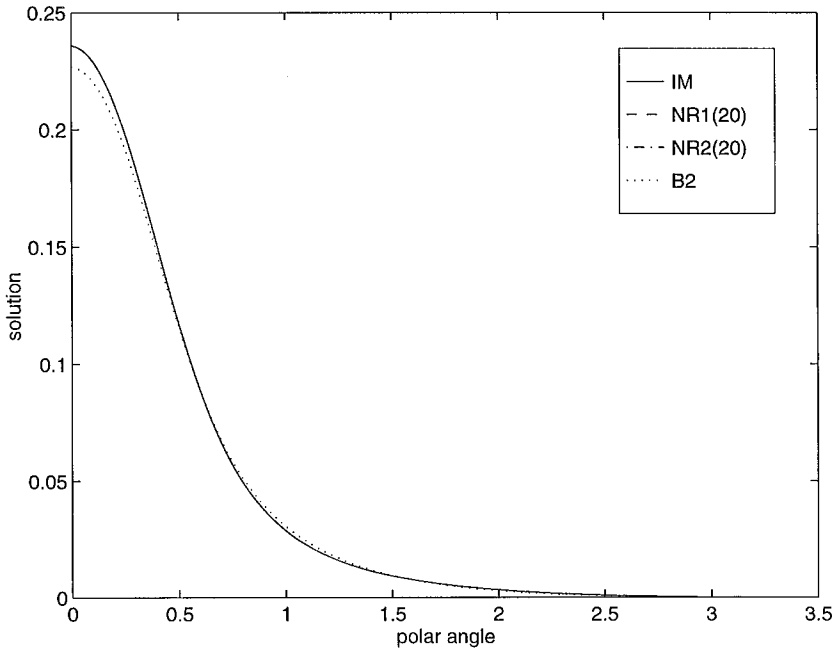


Figure 6. Solution profile at time $t = 10{\cdot}05$, and radius $r = 0{\cdot}75$ for $0 \leqslant \theta \leqslant \pi$, with a normalized frequency $\omega a/c = \pi/8$

$10^{-2}$ (not shown in the figure). For this frequency and value for $N$, the accuracy of NR1(20) and NR2(20) are nearly identical.

In Figure 4, we compare the maximum error at steady state obtained using NR1($N$) and NR2($N$), for $N$ increasing from 0 to 20. Results are given for four different computational domains positioned with truncation boundary at $R/a = 1{\cdot}5, 1{\cdot}75, 2{\cdot}0, 2{\cdot}5$, respectively. These results show the interplay between the number of terms used in NR1($N$) and NR2($N$), and the approximation to harmonic modes for $n > N$. Recall that NR2(0) and NR2(1) coincides with the local $B_2$ boundary condition, and NR1(0) is identical to $B_1$. NR1($N$) and NR2($N$) are both exact for all modes $n \leqslant N$. For harmonic modes $n > N$, NR2 approximates the solution with the local $B_2$ operator while NR1 approximates the solution with the local $B_1$ operator. Thus when using only a few terms in the truncated series for $N$, we expect NR2 to be more accurate than NR1.

As shown in Figure 4, solutions obtained using NR1($N$) and NR2($N$) all converge to a finite error value as $N$ is increased. This limiting error is controlled primarily by the boundary approximation of the term $(\mathbf{N}, Y_{nm})_\Gamma$ appearing in (32) and (34). The indirect formulation for NR2 also requires the evaluation of the surface gradient over the boundary which limits the accuracy. The results also show that when only a few terms $N$ are included, NR2($N$) yields more accurate results than NR1($N$) as expected. As the truncation boundary is moved farther away from the source, the number of terms $N$ required to obtain a fixed level of accuracy is reduced for both NR1 and NR2. For example, for NR2, and $R/a = 1{\cdot}5$, $N = 12$ terms are needed for the error to converge whereas, when $R/a$ is increased to 2·5, only $N = 5$ terms are needed to converge.

We finally compare the effect of decreasing frequency on the solution using NR2, NR1 and the local boundary condition $B_2$. In this study, a relatively low frequency of $\omega a/c = \pi/8$ is used with

 

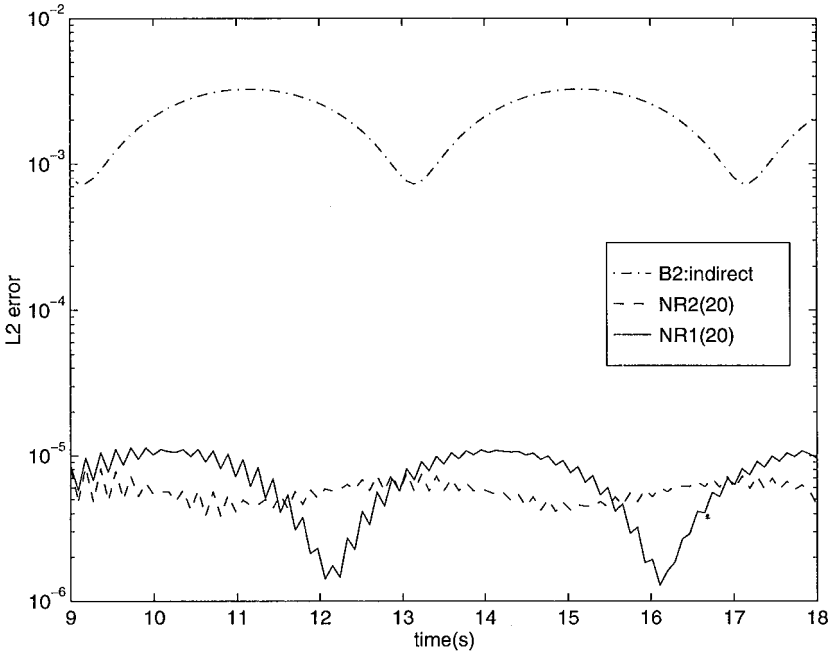


Figure 7. Instantaneous error $E(t)$ on the sphere $r = 0{\cdot}75$ due to a radiating piston with normalized frequency $\omega a/c = \pi/8$ and truncation boundary radius $R/a = 1{\cdot}75$. Results compared for boundary condition B2, NR1(20) and NR2(20). The error for B1 is approximately $10^{-2}$

a time step $\Delta t = 0{\cdot}015$. Figure 5 shows the time-histories at $\rho = 0{\cdot}75$, $\theta = 180°$, while Figure 6 compares the solution profile at $\rho = 0{\cdot}75$, at a fixed time $t = 10{\cdot}05$. The solution obtained using $B_2$ exhibits significant amplitude error at the difficult south pole region and also in the vicinity of the piston. In contrast, NR1(20) and NR2(20) shows excellent agreement with the infinite mesh solution throughout the computational domain.

Figure 7 shows the instantaneous error $E(t)$ at $\rho = 0{\cdot}75$. Comparing these results to Figure 3, we observe that the accuracy of both NR1(20) and NR2(20) improves by an order of magnitude as the frequency is reduced from $\omega a/c = \pi$ to $\omega a/c = \pi/8$. In the lower frequency case, the solution is smoother in the $\theta$ direction on the truncation boundary, resulting in a lower limiting error from the approximation of the inner product $(N, Y_{nm})_\Gamma$. In contrast, the accuracy of the local boundary operator $B_2$ tends to deteriorate as the frequency is reduced, as expected [4].

In Figure 8, we compare the maximum error at steady state obtained using NR1($N$) and NR2($N$), for $N$ increasing from 0 to 20, and with increasing truncation boundary $R/a$=1·5, 1·75, 2·0, 2·5. In contrast to the results shown in Figure 4 for the high-frequency case, as $R/a$ is increased, the error for both NR1($N$) and NR2($N$) converges to a lower limiting value. For the reduced frequency, with relatively smooth solutions in the circumferential co-ordinate, the error in the solution is dominated by the truncating of the infinite series in (32) or (34), and not the discretization error in the approximation to $(N, Y_{nm})_\Gamma$. Recall that for harmonic modes $n > N$, NR1(N) approximates the solution by eliminating leading terms up to $1/r^2$, while NR2(N) annihilates terms up to $1/r^4$. Therefore, as the truncating boundary radius $R$ gets larger, the error introduced by truncating the infinite series is smaller.

 

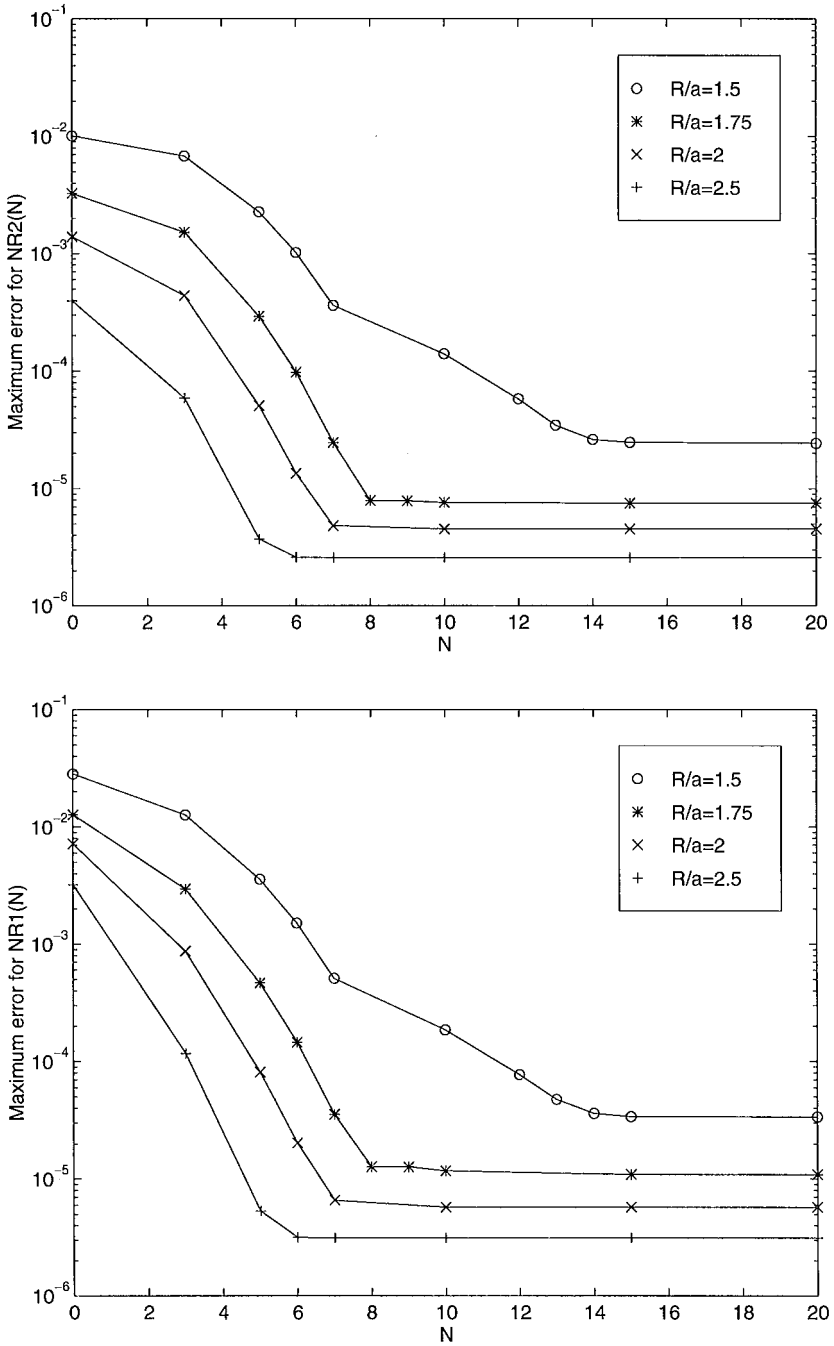


Figure 8. Maximum error measured at $r = 0{\cdot}75$ for the artificial boundary $\Gamma$ positioned at $R = 0{\cdot}75$ to $R = 1{\cdot}25$ and normalized frequency $\omega a/c = \pi/8$. (Top) NR2($N$) solution as a function of the number of terms $N$ included in the non-reflecting boundary condition. (Bottom) NR1($N$) solution as a function of the number of terms $N$ included in the non-reflecting boundary condition

 

## 6. CONCLUSIONS

A modified version of an exact non-reflecting boundary condition NR2($N$) first derived by Grote and Keller [6], is implemented in a finite element formulation for the scalar wave equation. The boundary condition may be viewed as an extension of the second-order local boundary operator $B_2$ derived by Bayliss and Turkel [2]. Two alternative implementations are given. In the first, the boundary operator is implemented directly as a 'natural' boundary condition in the variational equation. In the second, the operator is implemented indirectly by introducing auxiliary variables on the non-reflecting boundary $\Gamma$. Several versions of implicit and explicit time-integration schemes are presented for solution of the finite element semidiscrete equations concurrently with the first-order differential equations associated with the non-reflecting boundary condition and an auxiliary variable. Numerical computations demonstrate the disadvantage of the direct formulation for NR2($N$) caused by the difficulty in accurately approximating the radial derivative on the truncation boundary, and the resulting unsymmetric damping matrix. The indirect formulation using standard linear $C^0$ interpolation of NR2($N$) results in a symmetric system and accurate solutions.

Numerical studies were performed to compare the convergence properties of the NR1($N$) and NR2($N$) non-reflecting boundary conditions within the finite element formulation. The evolution of the error is measured in $L_2$ norm, and their behaviour as a function of the number of terms in the series $N$, and radial distance from the radiator/scatterer to the truncation boundary are compared. The results reported in this manuscript, together with other numerical examples performed by the authors [7, 8, 17, 18], demonstrate, that when implemented in the finite element method, both conditions are remarkably robust, and highly accurate, showing significant improvement in accuracy over the local $B_1$ and $B_2$ operators, especially as the truncation boundary is positioned near the source of scattering/radiation and for low frequencies. For a given level of accuracy, the non-reflecting boundary conditions give a large reduction in computer memory and execution time compared to the $B_2$ boundary condition. The results also show that when only a few terms $N$ are included in the series, NR2($N$) yields more accurate results than NR1($N$) as expected. As the truncation boundary is moved farther away from the source, the number of terms $N$ required to obtain a fixed level of accuracy is reduced for both NR1 and NR2.

ACKNOWLEDGEMENTS

We would like to thank NSF for funding this research via a Presidential Early Career Award for Scientists and Engineers (PECASE), and also Vincent Ervin for helpful discussions on the indirect implementation of the NRBC.

REFERENCES

1. Givoli D. Numerical methods for problems in infinite domains. *Studies in Applied Mechanics*, vol. 33. Elsevier: Amsterdam, 1992.
2. Bayliss A, Turkel E. Radiation boundary conditions for wave-like equations. *Communications in Pure and Applied Mathematics* 1980; **33**:707–725.
3. Pinsky PM, Abboud NN. Finite element solution of the transient exterior structural acoustics problem based on the use of radially asymptotic boundary operators. *Computer Methods in Applied Mechanics and Engineering* 1991; **85**: 311–348.
4. Thompson LL, Pinsky PM. A space-time finite element method for structural acoustics in infinite domains, Part 2: Exact time-dependent non-reflecting boundary conditions. *Computer Methods in Applied Mechanics and Engineering* 1996; **132**:229–258.

 

5. Grote MJ, Keller JB. Exact non-reflecting boundary conditions for the time dependent wave equation. *SIAM Journal of Applied Mathematics* 1995; **55**:280–297.
6. Grote MJ, Keller JB. Nonreflecting boundary conditions for time dependent scattering. *Journal of Computational Physics* 1996; **127**:52–65.
7. Thompson LL, Huan R. Accuracy of Nonreflecting Boundary Conditions for the Time-Dependent Wave Equation, Mathematical and Numerical Aspects of Wave Propagation. In *Proceedings of the Fourth International Conference on Mathematical and Numerical Aspects of Wave Propagation*, De Santo JA (ed.), SIAM, 1998.
8. Thompson LL, Huan R. Implementation of exact non-reflecting boundary conditions in the finite element method for the time-dependent wave equation. *Computer Methods in Applied Mechanics and Engineering*, to appear.
9. Lamb H. *Hydrodynamics*. (4th edn). Cambridge University Press: Cambridge, 1916: 517, equation (4).
10. Kallivokas LF, Bielak J, MacCamy RC. Symmetric local absorbing boundaries in time and space. *Journal of Engineering Mechanics* ASCE 1991; **117**:2027–2048.
11. Newmark NM. A method of computation for structural dynamics. *Journal of Engineering Mechanics Division* ASCE 1959; 67–94.
12. Hughes TJR. A precis of developments in computational methods for transient analysis. *Journal of Applied Mechanics* 1983; **50**:1033–1040.
13. Butcher J. *The Numerical Analysis of Ordinary Differential Equations*. Wiley: New York, 1987.
14. Cook RD, Malkus DS, Plesha ME. *Concepts and Applications of Finite Element Analysis*. (3rd edn). Wiley: New York, 1989.
15. Friedlander FG. On the radiation field of pulse solutions of the wave equation. *Proceedings of the Royal Society of London* 1962; **A 269**:53–65.
16. Morse PM, Feshbach H. *Methods of Theoretical Physics*, vol. II. McGraw-Hill: New York, 1953.
17. Thompson LL, Huan R. Exact non-reflecting boundary conditions for transient radiation in semi-infinite regions. Technical Report CMCU-98-02, November (1998), Computational Mechanics Lab, Clemson University. Submitted to the *Journal of the Acoustical Society of America*.
18. Thompson LL, Huan R. Computation of far-field solutions based on exact nonreflecting boundary conditions for the time-dependent wave equation. Technical Report CMCU-98-03, November (1998), Computational Mechanics Lab, Clemson University. Submitted to *Computer Methods in Applied Mechanics and Engineering*.

 